In Situ Gamma Irradiation Effects on 4H-SiC Bipolar Junction Transistors

Alex Metreveli, Anders Hallén, Ilaria Di Sarcina, Alessia Cemmi, Jessica Scifo, Adriano Verna, and Carl-Mikael Zetterling, *Fellow, IEEE*

Abstract— Gamma irradiation effects have been investigated on 4H-silicon carbide (SiC) bipolar junction transistors (BJTs), where the devices were exposed under different biasing regimes such as saturation, cut-off, active, reverse, and zero bias. Since bipolar transistors can be affected by dose rate, three different dose rates were used during irradiation tests. Characterization was performed on the transistors, without irradiation but in situ to avoid delays between irradiation and characterization. The study explores the relationship between biasing conditions and their impact on radiation-induced degradation of SiC BJT transistors. From these experiments, it is clear that 4H-SiC bipolar transistors can withstand high gamma doses, in the worst case less than 22% degradation of the current gain was seen for doses of up to 2 Mrad(Si).

Index Terms— Bipolar transistor, Co-60, critical regime, enhanced dose-rate sensitivity, gamma radiation, silicon carbide (SiC).

I. Introduction

THE increasing demand for electronics in specialized applications such as space, military, and nuclear reactors has called for robust semiconductor device technology that can sustain high temperatures and radiation exposure. However, the prevalent silicon-based devices are less suited for these environments due to the inherent limitations of the semiconductor material. Silicon carbide (SiC), a wide bandgap semiconductor, is an attractive choice for harsh environments due to its low intrinsic carrier concentration, higher critical electrical field, and thermal conductivity and, last but not least, inherent radiation hardness.

Being one of the suitable materials for radiation environments, such as space, it is imperative that SiC-based devices are qualified for radiation hardness. In this regard, several researchers have reported high tolerance of SiC devices and circuits against gamma-rays up to 332 Mrad [1], [2], [3]. However, it is worth pointing out that, in report [1], [2], the tested devices are kept unbiased during the irradiation tests.

This does not fully emulate the real-life scenario, where the devices under tests (DUTs) are operating during the exposure.

Hence, in the present work, we investigated the dose effects on SiC bipolar junction transistors (BJTs) that were irradiated while operating in different regimes such as saturation, cut-off, active, reverse, modes and zero-bias, for a full picture. Moreover, the impact of exposure rate on the degradation of the BJTs current gain values is also investigated extensively.

In anticipation of potential enhanced dose rate sensitivity, we opted to conduct an additional investigation of transistors behavior under different exposure rates. This effect is known in silicon devices and refers to the phenomenon of additional radiation-induced degradation at lower dose rates compared to high dose rates. This effect is particularly relevant in space, since the natural gamma radiation background is low, compare to the terrestrial sources.

It is found that the devices are significantly more tolerant in the active regime, irrespective of the exposure rate. This contrasts with the severe degradation that the devices experience when they are irradiated in an unbiased mode. These results indicate a superior radiation hardness of the SiC BJTs than reported previously [1], [2] and suggest that the devices in radiation-prone environments can have improved reliability if they are provided with biasing rather than unbiased during standby mode.

II. Experimental Methods

A. Device and Circuit Fabrication

Discrete bipolar transistors were fabricated on a 100 mm 4H-SiC wafer provided by CREE.[1] The wafer consisted of six epitaxially grown layers with different doping. The recipe used to fabricate the BJTs was similar to the one reported in [1], [2], and [4], with the exception of the two top-level interconnections required for the circuits. In the previous batch, the metal interconnections were made up of Al [1], [2], whereas TiW/Al was used for both the interconnection levels in the present batch.

All devices were electrically isolated from each other and placed at a significant distance to minimize mutual interference. The cross section of the device and its top view are illustrated in Fig. 1(a) and (b), respectively.

The improved metallization process leads to lower contact resistances and, hence, better current gain values in the low
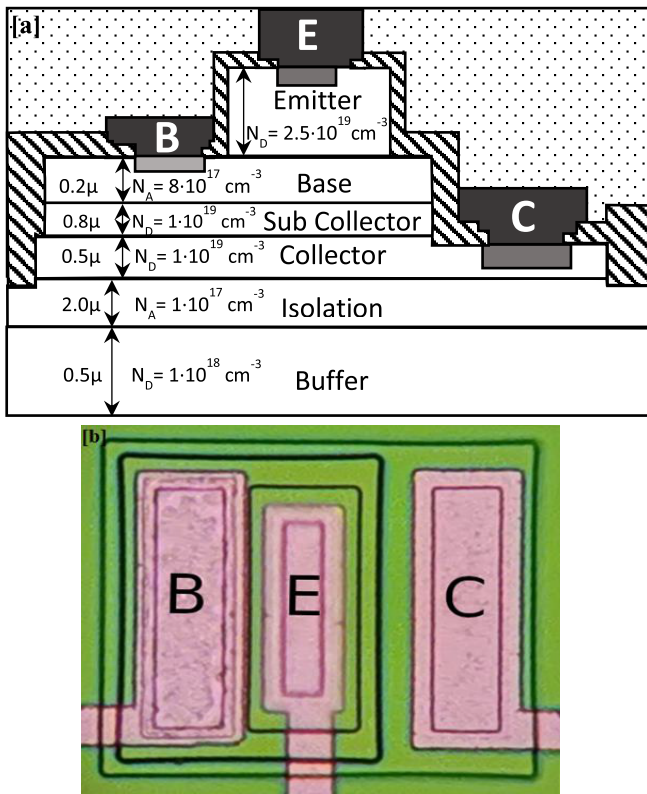
[1]Registered trademark.

Fig. 1. Cross section of the device, with the substrate and the different epitaxial layers. (a) View from the top. (b) Not to scale.

injection regime. The gain of the devices discussed in the article varies from 88 up to 102.

The devices were packaged for the radiation tests. All the chips used in the irradiation experiments were mounted in Kyocera[1] 40 pin dula in-line package (DIP) and bonded by gold wires. All the processing steps from the wafer till final measurements were made at Electrum laboratory at KTH.

B. Irradiation

Gamma radiation tests were performed at the ^{60}Co Calliope facility at ENEA Casaccia Research Center, Rome (Italy). The Calliope is a pool-type irradiation facility equipped with a ^{60}Co -source in a high volume (7.0 × 6.0 × 3.9 m) shielded cell. The maximum licensed activity for the Calliope facility is $3.7 × 10^{15}$ Bq (100 kCi) and the current activity (May 2023) is $1.4 \, 10^{15}$ Bq (38 kCi). The plane source rack is composed of 25 ^{60}Co source rods with an active area of 41 × 75 cm.

The radiation consists of two photons of 1.17 and 1.33 MeV (mean energy of 1.25 MeV), hence the irradiated material is not activated and it can be safely manipulated immediately after the end of the irradiation test. At the Calliope facility several dosimetric systems are available, for BJTs irradiation tests the ESR-alanine dosimetry was used [5].

C. Measurement Procedure

The measurements were performed according to the semi-conductor device testing standards, namely, MIL-STD-883L and MIL-STD-750 (Method 1019.9) [6], [7]. In order to gauge

the effects of gamma radiation on the SiC devices in real-time, a remote measurement setup was designed such that they could be exposed while they are operating in saturation, cut-off, active, reverse, and zero-bias regimes, as well as characterized in situ immediately after each exposure. This method is more reliable and better represents the radiation environment when compared to a previous report on the gamma tolerance of SiC devices [1], [2]. In [1], [2], the device terminals were left floating during exposure and there was a significant time gap between the exposure and measurements.

The electrical tests were performed using a setup based on National Instruments[2] measurement equipment assembled using NI PXIe-1078 chassis with PXIe-4081 digital multimeter (DMM), two PXIe-4136 source measure units (SMUs), a programmable PXI-4110 dc power supply, and a NI PXIe-2532 switching matrix. Due to the high exposure rate in the vicinity of the chamber, the measurements were performed remotely using 20 m cables with extra shielding biased to the guard terminals of the SMUs to reduce parasitic capacitance and noise induced by the radiation source in the cable shielding.

The measurement program switching matrix was assembled for long lines using sense mode on the measurement units.

The line calibration was performed on each iteration of the die measurement. Due to the multiple tests and line self-calibration for better precision, the measurements of the devices took 2 min after each exposure. The iteration time was adjusted so that the exposure time was at least ten times longer than the measurement time.

A common option to measure the dc characteristics of transistors is described in [8], hence in actual practice a more common method is used and described below in the next paragraph.

The setup was programed to perform dc measurements, such as Gummel and I_C–V_{CE} curves, using a sense configuration method [9]. During the measurement, V_{CE} was set to 15 V while V_{BE} was swept from 0 to 15.6 V with a step of 0.2 V for the Gummel plot. The current compliance had been set up to 1 A_{dc} for each of the terminals. To avoid induced noise, the measurement code was written such that all the voltage and currents at each V_{BE} were measured seven times and then a trimmed mean ($\alpha = 15\%$) was taken. This method helps in increasing the resolution up to 5 ± 1 nA on 20 m non-coaxial cables, which we found satisfactory.

The dc characteristics of the SiC BJTs were measured at a wide range of gamma-ray doses [7.5 rad(Si) to 20 Mrad(Si)], and at different dose rates: low dose rate LDR = 9.975 rad(Si)/s, normal dose rate NDR = 45.26 rad(Si)/s and high dose rate HDR = 124.5 rad(Si)/s. Moreover, to achieve a spectrum that better emulates the space environment, a low-energy secondary photon component was removed by using an Al/Pb filter as it is not observed in space.

For HDR and NDR and all the operational regimes at least two devices were tested. Once the critical regime was determined, we further increased the reliability of the results by testing at least two additional devices. By considering
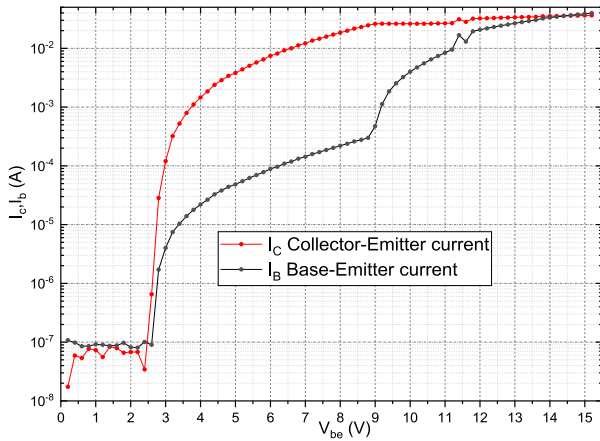
[2]Trademarked.

Fig. 2. Gummel plot of the fabricated 4H-SiC.

TABLE I
OPERATIONAL REGIMES DURING THE EXPOSURE

Terminal	Parameter	Saturation	Cut-off	Active	Reverse	Zero-bias	Un-bias [1]
Emitter	V_{Emit}	0					float
	I_{Emit}	adj up to I_{bmax}				0	float
Collector	V_{Coll}	30% V_{cc}	V_{cc}			0	float
	I_{Coll}	adj up to I_{bmax}				0	float
Base	V_{Base}	adj		50% V_{cc}	0		float
	I_{Base}	85% I_{bmax}	adj up to 10% I_{bmax}	50% I_{bmax}	adj up to 10% I_{bmax}		float

the outcomes and correlation between HDR and NDR cases, we successfully identified the critical regime for the LDR case.

All the extra sample tests were made to increase the reliability of the results.

For HDR and NDR cases all the samples were exposed at least up to 1 Mrad(Si) and for the critical bias condition up to 12 Mrad(Si). For the LDR case, the dose rangers were at least 550 rad(Si) and 2 Mrad(Si), respectively.

D. Initial Measurement Results

Fig. 2 illustrates a representative Gummel plot of the BJT before irradiation. The transistor expectedly turns on at $V_{BE} = 2.35–2.6$ V, after which both I_C and I_B increase exponentially. However, a sharp increase in I_B is observed at $V_{BE} = 6.2–10$ V, which is attributed to the emitter current crowding effect and correlates to the processing variation.

Due to the 2-D structure of the BJT, the base current creates a lateral voltage drop between the base contact region and the center of the emitter contact. As the current density rises exponentially with increasing V_{BE}, the current density at the base contact becomes much larger when compared to the density at the center of the emitter contact [10]. The current crowding effect is more severe in BJTs where: 1) the base resistance is high; 2) the emitter width is large; and 3) only a single base contact is used which promotes the lateral voltage drop between the BE and emitter contact region. The BJT design used in this study has a single base contact to reduce the device footprint, thereby causing the current crowding effect.

This phenomenon is also observed in previously reported SiC BJTs with a single base contact [11], [12]. Moreover, the exact V_{BE} value at which the current crowding effect begins to dominate, depends on the emitter geometry, which can vary slightly from one device to another on the same wafer due to variations in the etching process.

III. RESULTS AND DISCUSSION

To investigate the gamma radiation effects, the SiC BJT was connected in a common emitter configuration. This BJT configuration was chosen over others as it is used commonly in digital and analog circuit applications. The operating regimes

under which the BJT was irradiated and characterized, include saturation, cut-off, active, reverse, and the "zero-bias" modes, where all three terminals of the BJT are connected to the ground.

The operating regimes of BJTs during the exposure are described in Table I. V_{CC} was set to 15 V (Sense mode), while I_{bmax} had the values 26–40 mA (maximum current in the base cable). The term "adj" refers to the auto-tuning of the SMU in a mode that compensates for losses and induces noise in long lines and maintains a specified parameter.

For the cases presented below, the most typical sample behavior was selected, plotted, processed, and based on it, beta characteristics were constructed. Maximum beta values were taken from the meddle state regime of BJT ($V_{CE} = 15$, $V_{BE} = 3.2–9$ V).

A. Saturation Regime (Digital On)

Fig. 3 shows the dose effects [up to ∼1 Mrad(Si)] on the BJT Gummel plot when the device is biased in saturation mode during the exposure.

The exposure rate in this case is 124.5 rad(Si)/s. As evident from the figure, gamma irradiation exposure causes the base current (I_B) to increase and the collector current (I_C) to decrease. The I_C is most sensitive to the dose at low V_{BE} voltages as the result of field variation in the base–emitter region under the effect of induced charge in the oxide and SiC/SiO$_2$ interface, whereas the degradation in I_B is mostly uniform with respect to V_{BE}.

These changes in the collector and base currents due to the absorbed dose translate to a degradation in the maximum current gain of the transistor, according to Fig. 3(b).

The biggest drop in the current gain is in the first iteration of exposure which correlates to the Hydrogen model of oxide degradation [13], [14], [15], [16], [17].

In addition to the total absorbed dose, the BJT current gain is also sensitive to the gamma exposure rate. Fig. 4 illustrates the dose effects on the normalized BJT current gain for different exposure rates, namely 9.975 rad(Si)/s (LDR), 45.26 rad(Si)/s (NDR), and 124.5 rad(Si)/s (HDR), where the exposure for all three dose rates is performed when the BJT
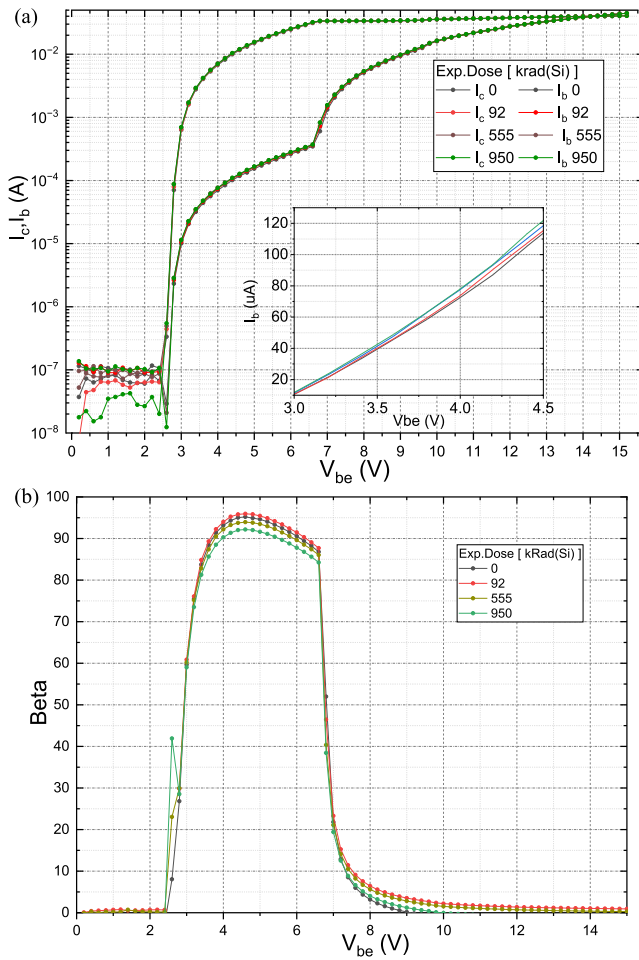
Fig. 3. Dose effects for the BJT in saturation regime during the exposure. (a) Gummel plot. Sub plot base current (I_b) in $V_{be} = 3$–4.5 V. (b) Current gain (Beta) characteristic curve.
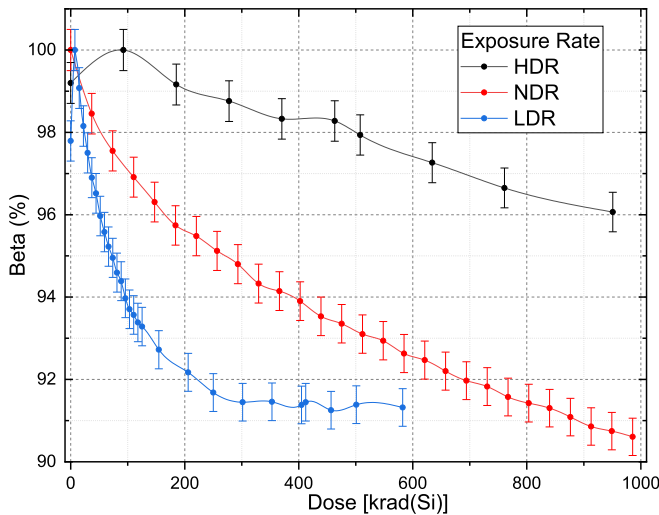

Fig. 4. Effect of dose and dose rate on the normalized BJT current gain in Saturation mode.

is in the saturation regime. The pre-exposure current gain for the devices exposed at LDR, NDR, and HDR, are 93, 103, and 94, respectively. As observed from the Fig. 4, the BJT exposed at the low rate degrades faster than NDR and HDR cases at the same total absorbed dose.
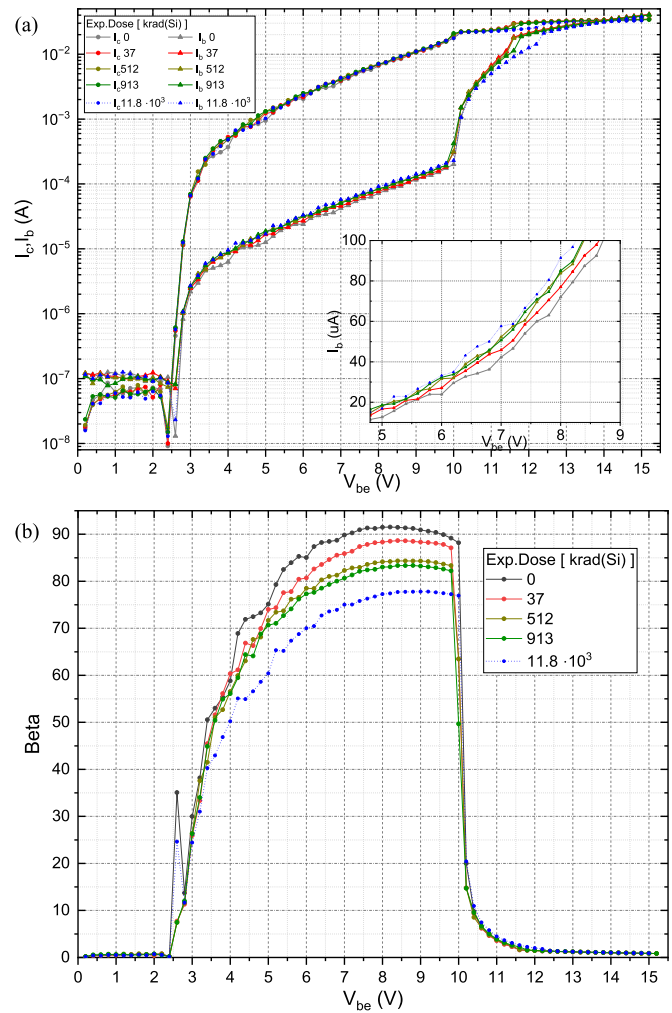

Fig. 5. Dose effects in the cut-off regime during the exposure. (a) Gummel plot. Sub plot base current (I_b) in $V_{be} = 5$–9 V. (b) Current gain (Beta) characteristic curve.

No further degradation is observed after a dose of 300 krad(Si). On the other hand, the BJT exposed to NDR continues to degrade as the dose increases, and the device exposed to HDR is most resistant to the total absorbed dose.

However, it is worth pointing out that the current gain degradation does not exceed 10% at any exposure rate, even at absorbed dose of 1 Mrad, demonstrating the superior radiation tolerance of the devices in saturation mode.

B. Cut-Off Regime (Digital Off)

Fig. 5(a) and (b) shows the dose effects [up to ~ 1 Mrad(Si)] on the BJT performance when the device is exposed in cut-off mode, at an exposure rate of 124.5 Mrad(Si)/s. As demonstrated in Fig. 5(a), the radiation impact on I_C at low V_{BE} is negligible, while a uniform degradation in I_B is observed at medium V_{BE}. At high V_{BE}, the large shift in currents is potentially attributed to the induced charges at the SiC/SiO₂ interface. The dose rate effects for the BJT exposed in cut-off mode are shown in Fig. 6.

The pre-exposure current gain for the devices exposed at LDR, NDR, and HDR, are 94, 86, and 84, respectively. Unlike the saturation regime, the BJTs exposed in the cut-off mode
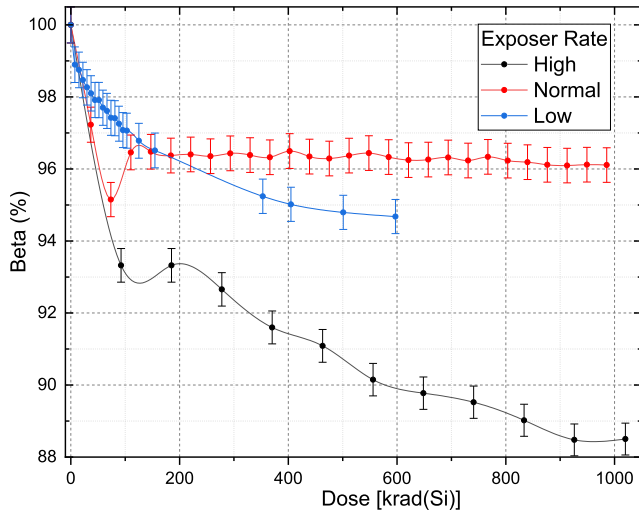
Fig. 6.   Effect of dose and dose rate on the normalized BJT current gain in cut-off mode.

are most sensitive to high exposure rates where the current degrades by more than 10% at a dose of 600 krad(Si).

The low and normal exposure rates do not induce much damage to the BJTs as the current gain degradation is less than 6% for both dose rates.

C. Active Regime (Amplification)

The active regime is one of the most interesting due to its application in analog amplifiers. Fig. 7(a) and (b) shows the behavior of the transistor under exposure in the active regime. Fig. 8 shows the beta behavior under different exposure rates in the active regime. We see that the resistance of the base changes significantly at high V_{BE}. It is also obvious how the "knee" has shifted to around 7–8 V, indicating an additional impact of induced charges at the SiC/SiO$_2$ interface in the base region. From Fig. 7(b), it is also evident that the width of the current gain region shrunk. This phenomenon should be taken into account in amplification IC designs for space applications. Such dynamics of currents and current gain gives a hint that the accumulated induced charge in this regime is negative.

D. Reverse Regime

The reverse regime is not critical from an application viewpoint; however, to provide a complete picture of the gamma exposure on the operating regime, the results are presented in Figs. 9 and 10. The behavior of current degradation is similar to the active regime, but with a positively induced trapped charge in the SiO$_2$. The deviation in current gain was the smallest one for this regime. The dependence of dose rate is shown in Fig. 10.

E. Zero-Bias Regime

Finally, the zero-bias regime showed the largest deviation from the initial values. Fig. 11(a) and (b) is for 124.5 rad(Si)/s dose rate, while Fig. 11(c) is for 9.975 rad(Si)/s. From Fig. 11(a) and (c), it is observed that the base degradation is always significant above turn-on ($V_{BE} = 2.5$ V), especially at
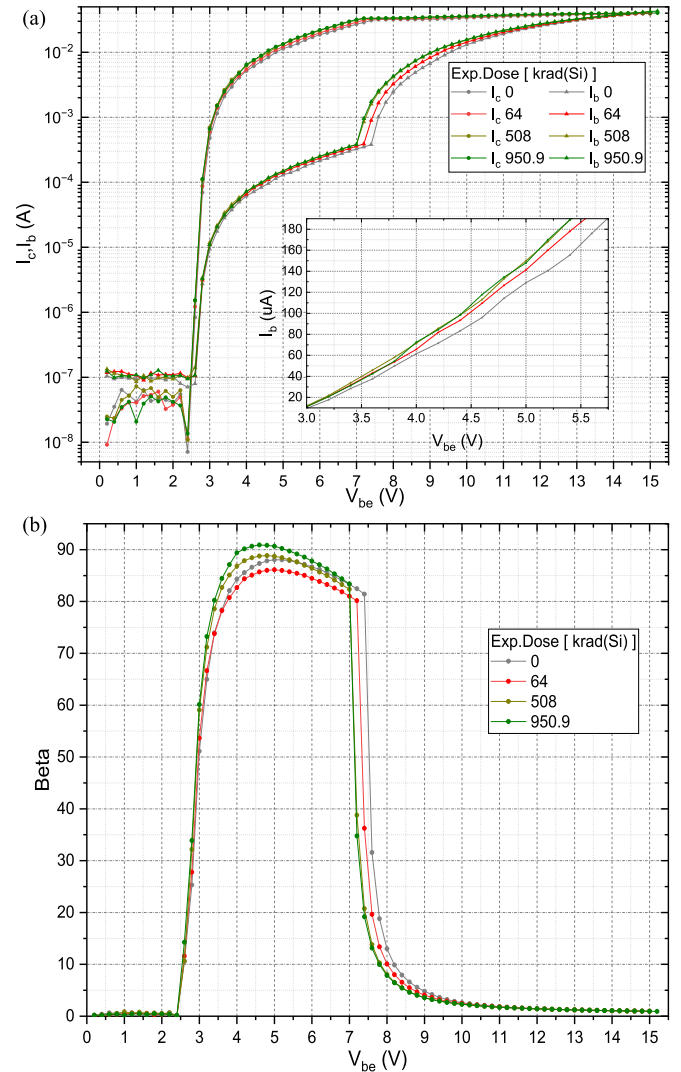

Fig. 7.   Dose effects on the BJT current gain in active regime during the exposure. (a) Gummel plot. Sub plot base current (I_b) in $V_{be} = 3$–4.5 V. (b) Current gain (Beta) characteristic curve.
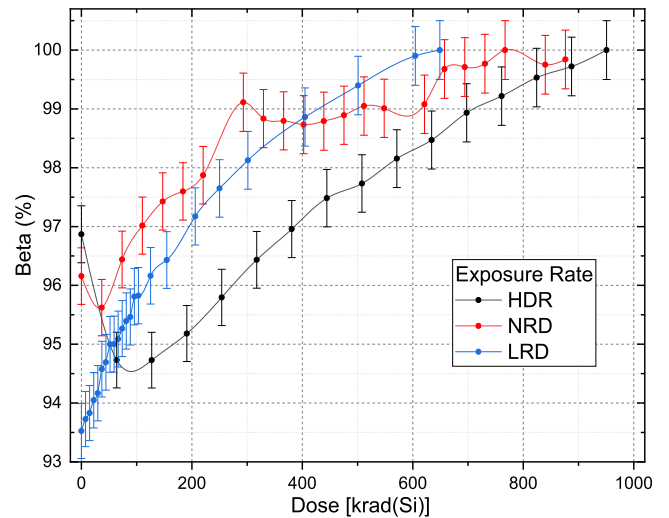

Fig. 8.   Normalized behavior due to the exposure rate in active regime.

the high injection level. It is interesting how the characteristic "knee" had changed between 10 and 11 V. Such behavior shows the additional impact of the induced charge. The dual
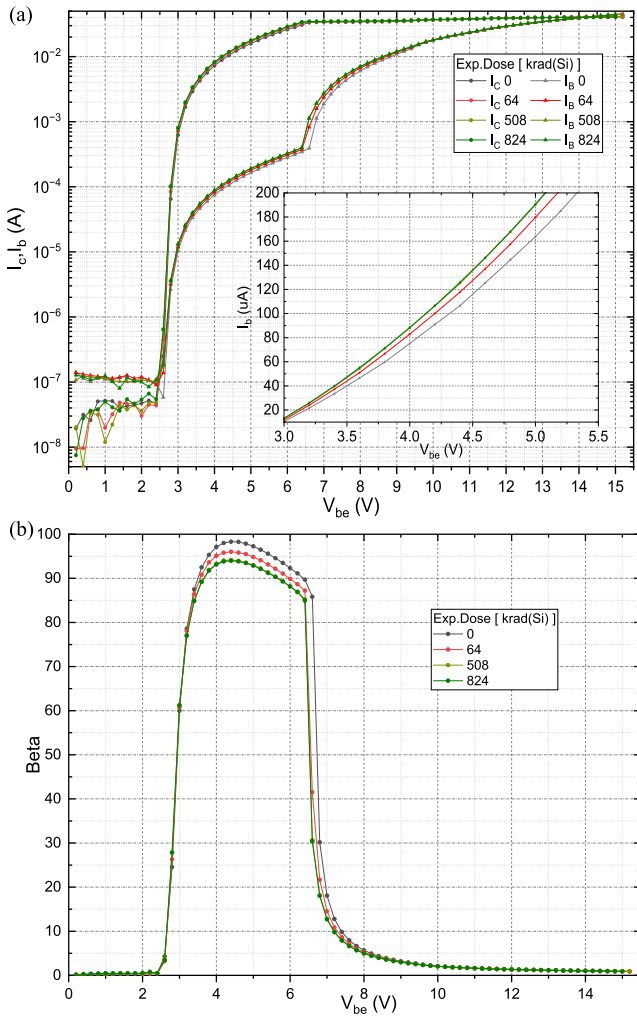
Fig. 9. Dose effects in cut-off regime during the exposure. (a) Gummel plot. Sub plot base current (I_b) in V_{be} = 3–4.5 V. (b) Current gain (Beta) characteristic curve.

Fig. 11. Dose effects in the zero-bias regime during the exposure. (a) Gummel plot. Sub plot base current (I_b) in V_{be} = 3–7 V. (b) Current gain (Beta) characteristic curve.

reduced. Figs. 11(b) and 12 illustrate that the current degradation in this regime was the worst among all investigated cases, particularly for the lowest dose rate.

IV. SUMMARY OF DOSE RATE EFFECTS

Fig. 13 shows the distribution of all irradiated samples with respect to the dose rate and operating regime. On the Y axes the normalized beta deviation values are presented. Some of the samples got index E, meaning they had been exposed under mentioned conditions, but without remote measurement.

As observed from the distribution, zero-biasing shows the largest deviation from the initial values, followed by the saturation regime, which is common in logic BJT devices. Cut-off, active, and reverse regimes show similar degradation up to 6% on the current gain values. For all operating modes, a correlation between the dose intensity and the mentioned parameter is evident.

The deviation dispersion was larger under HDR, while the scatter was reduced under LDR conditions. In the critical regime, it is evident that the average deviation shifts toward greater degradation under low-intensity conditions.
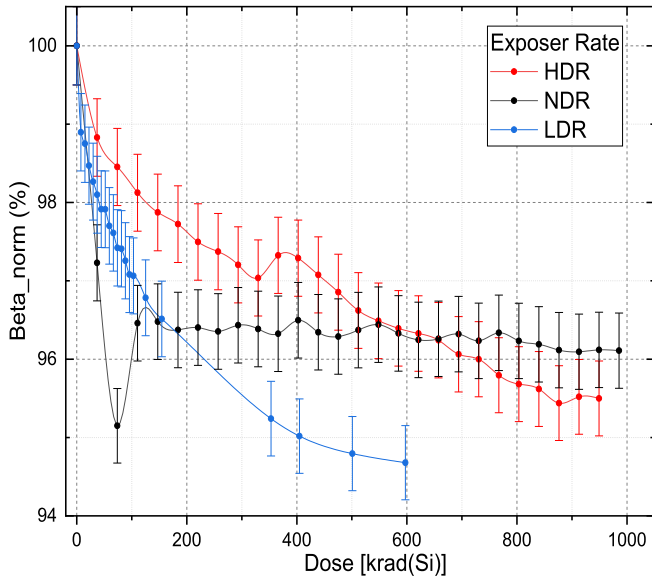

Fig. 10. Normalized Degradation due to the exposure rate for the Reverse bias regime.

"knee" characteristics are attributed to the additional current spread via the surface of the transistor [16]. It is clear that the slope had decreased, which means that the resistance was
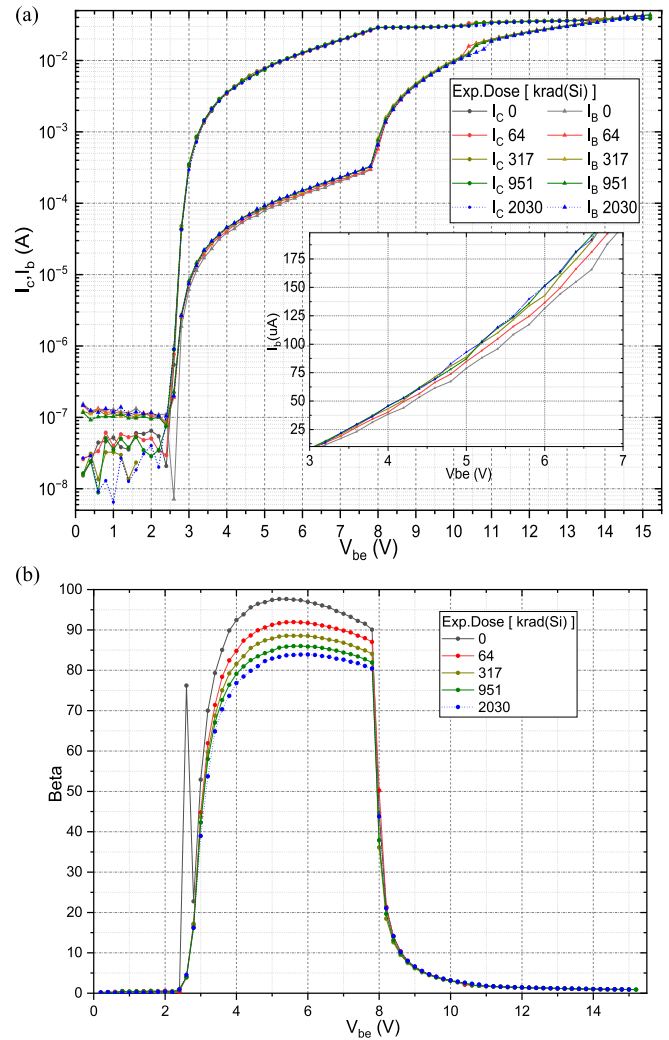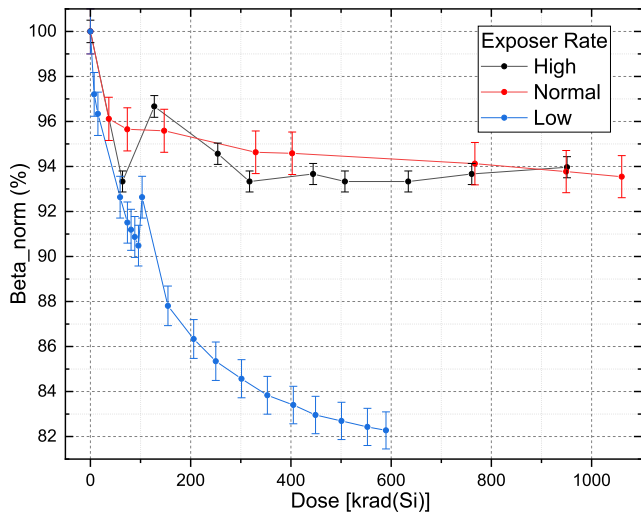
Fig. 12. Normalized degradation due to the exposure rate for zero-bias regime.
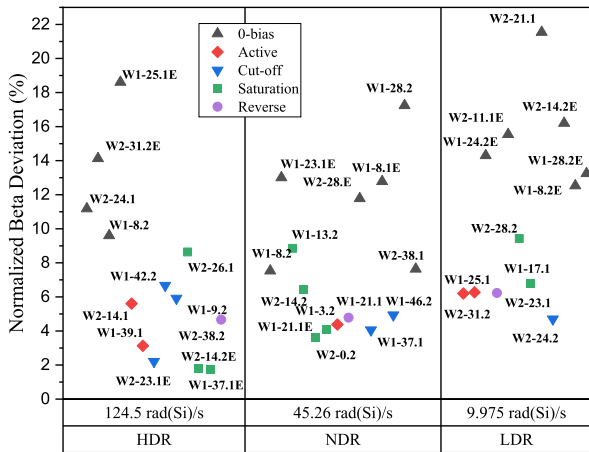

Fig. 13. Degradation distribution of irradiated samples for different dose rates and operating regimes.

This observation suggests a similarity in the induced charge migration processes within the silicon oxide [17], [18].

The mean deviation values for "zero-bias" were found to be for HDR 12.2 (HDR), 12.5 (NDR), and 15.5 (LDR). Even for non-critical regimes, there is a dose rate correlation: at a high rate, the spread in the final values is large, while with a decrease in the rate, the values become more uniform. Thus, it is suggested that it is more appropriate to use moderate, or low-rate exposure rates for the BJTs.

Furthermore, a closer look at the current gain behavior (Figs. 4, 6, 8, 10, and 12), reveals that there is a peak after the first exposure in almost all the cases, after which the values start to decrease in a stable manner till saturation.

Such peaks indicate that the induced charge formation process in the oxide proceeds in a non-stationary way, as is described for Si. For Si, a small impact of induced charge per photon on the electron and hole velocities is commonly observed, as described by the model in [14], [15], [16], [17], and [18]. This model suggests that, under HDR conditions, induced charge affects the velocity of holes and slows them down such that do not reach the Si/SiO$_2$ interface efficiently

TABLE II
DEGRADATION BEHAVIOR OF THE CURRENTS DURING THE EXPOSURE

V_{BE}		Current	Regime					
State	Voltage (V)		Saturation	Cut-off	Active	Reverse	Zero bias	Un-bias [1]
Low	0–3.5	I_C	↑↑	–	↑↑	↑↑	↓	↑↑
		I_B					↑↑	
Med	3.5–(6.5÷9)*	I_C	–	–	↑↑	↑	–	↓
		I_B	↑↑	↑↑		↑↑	↑↑↑	–
High	9–15	I_C	→→	–			↘↘	No Data
		I_B	→	→→	←←←	←		

Minor (↑), moderate (↑↑), significant (↑↑↑) increments, minor (↓) reduction. Minor (→), moderate (→→) shift to higher V_{be} values, moderate (←←), significant (←←←) shift to lower V_{be} values, moderate(↘↘) reduction with shift to higher V_{be}, (−) No significant change. * − Voltage distribution correlates to the processing variation of the samples.

when compared to LDR conditions [17]. This degradation process is stable, till it reaches the specification range or goes to saturation and eventually rebounds. For SiC MOS structures the degradation mechanism is slightly different.

We observe a significant drop in current gain first iterations. No matter which dose rate is used, the initially trapped protons accumulate at the SiC/SiO$_2$ interface which disturbs the G-R balance initially after which it becomes stable in further iterations.

We assume that this phenomenon could be explained by the significant incorporation of Carbon on the "Si-face." For the SiC/SiO$_2$ interface we expect a higher amount of build-in positive charge. That causes a difference in the hole migration behavior within the oxide region compare to Si model.

Unfortunately, due to the harsh environment and long lines C–V measurement techniques could not be applied. Therefore, at present, we are attempting to simulate the degradation process of mentioned SiC bipolar transistors.

The degradation behaviors are summarized in Table II.

V. CONCLUSION

In this article, we have investigated the effects of gamma radiation total dose and dose rate on SiC BJTs. To emulate the operating conditions of the devices in space, the BJTs were biased during the exposure. All five operating regimes, i.e., saturation, cut-off, active, reverse, and zero bias were investigated in addition to the floating regime [1], [2]. The results show (Fig. 13) that BJTs biased in zero-biased mode are the most sensitive to gamma radiation exposure. The biggest gain degradation (up to 22%) had been achieved at 2 Mrad(Si). The second worst mode is saturation (Digital On). The degradation was below 10% even for the dose up

to 1 Mrad. Enhanced dose rate sensitivity has been registered [18]. That proves that SiC behavior is similar to Si from this perspective.

ACKNOWLEDGMENT

The authors would like to thank Giuseppe Ferrara for technical support.

REFERENCES

[1] S. S. Suvanam, "Radiation hardness of 4H-SiC devices and circuits," Ph.D. dissertation, KTH Roy. Inst. Technol., 2017. [Online]. Available: https://www.diva-portal.org/smash/get/diva2:1066193/FULLTEXT02

[2] S. S. Suvanam et al., "High gamma ray tolerance for 4H-SiC bipolar circuits," *IEEE Trans. Nucl. Sci.*, vol. 64, no. 2, pp. 852–858, Feb. 2017, doi: 10.1109/TNS.2016.2642899.

[3] P. Beck et al., "Radiation evaluation of digital isolators for space applications," in *Proc. 17th Eur. Conf. Radiat. Effects Compon. Syst. (RADECS)*, Geneva, Switzerland, Oct. 2017, pp. 413–417, doi: 10.1109/RADECS.2017.8696248.

[4] S. Roy et al., "Silicon carbide bipolar analog circuits for extreme temperature signal conditioning," *IEEE Trans. Electron Devices*, vol. 66, no. 9, pp. 3764–3770, Sep. 2019, doi: 10.1109/TED.2019.2928484.

[5] S. Baccaro, A. Cemmi, I. Di Sarcina, and G. Ferrara, "Gamma irradiation Calliope facility at ENEA," Casaccia Res. Centre, ENEA, Rome, Italy, Tech. Rep. RT/2019/4/ENEA, 2018. [Online]. Available: https://www.enea.it/it/seguici/pubblicazioni/pdf-opuscoli/calliope.pdf

[6] NASA. (2018). *MIL-STD-883K Test Method Standard Microcircuits W/Change 3*. [Online]. Available: https://s3vi.ndc.nasa.gov/ssri-kb/static/resources/MIL-STD-883K_CHG-3.pdf

[7] NASA. (2016). *MIL-STD-750F (Test Methods for Semiconductor Devices) W/Change 2*. [Online]. Available: https://s3vi.ndc.nasa.gov/ssri-kb/static/resources/MIL-STD-750F_CHG-2.pdf

[8] L. Zhu, K. Vafai, and L. Xu, "Modeling of non-uniform heat dissipation and prediction of hot spots in power transistors," *Int. J. Heat Mass Transf.*, vol. 41, no. 15, pp. 2399–2407, Aug. 1998.

[9] L. Zhu, K. Vafai, and L. Xu, "Modeling of non-uniform heat dissipation and prediction of hot spots in power transistors," *Int. J. Heat Mass Transf.*, vol. 41, no. 15, pp. 2399–2407, Aug. 1998, doi: 10.1016/S0017-9310(97)00299-8.

[10] S. Hou, "Silicon carbide high temperature photodetectors and image sensor," Ph.D. dissertation, KTH Roy. Inst. Technol., Stockholm, Sweden, 2019. [Online]. Available: https://www.diva-portal.org/smash/get/diva2:1303493/FULLTEXT01.pdf

[11] L. Lanni, "Silicon carbide bipolar technology for high temperature integrated circuits," Ph.D. dissertation, Dept. Elect. Eng. (EECS), KTH Royal Inst. Technol. Stockholm, Stockholm, Sweden, 2014. [Online]. Available: http://www.diva-portal.org/smash/record.jsf?pid=diva2:482731

[12] M. Shakir, "Process design kit and high-temperature digital ASICs in silicon carbide," Ph.D. dissertation, KTH Roy. Inst. Technol., Stockholm, Sweden, 2019. [Online]. Available: https://www.diva-portal.org/smash/get/diva2:1317122/FULLTEXT01.pdf

[13] *Low-Level Measurements Handbook*, 7th ed., Keithley, Cleveland, OH, USA. [Online]. Available: https://download.tek.com/document/LowLevelHandbook_7Ed.pdf

[14] S. C. Witczak, R. C. Lacoe, D. C. Mayer, D. M. Fleetwood, R. D. Schrimpf, and K. F. Galloway, "Space charge limited degradation of bipolar oxides at low electric fields," *IEEE Trans. Nucl. Sci.*, vol. 45, no. 6, pp. 2339–2351, Dec. 1998.

[15] D. M. Fleetwood, L. C. Riewe, J. R. Schwank, S. C. Witczak, and R. D. Schrimpf, "Radiation effects at low electric fields in thermal, SIMOX, and bipolar-base oxides," *IEEE Trans. Nucl. Sci.*, vol. 43, no. 6, pp. 2537–2546, Dec. 1996.

[16] D. M. Fleetwood et al., "Physical mechanisms contributing to enhanced bipolar gain degradation at low dose rates," *IEEE Trans. Nucl. Sci.*, vol. 41, no. 6, pp. 1871–1883, Dec. 1994.

[17] D. M. Fleetwood, R. D. Schrimpf, S. T. Pantelides, R. L. Pease, and G. W. Dunham, "Electron capture, hydrogen release, and enhanced gain degradation in linear bipolar devices," *IEEE Trans. Nucl. Sci.*, vol. 55, no. 6, pp. 2986–2991, Dec. 2008, doi: 10.1109/TNS.2008.2006485.

[18] H. P. Hjalmarson et al., "Mechanisms for radiation dose-rate sensitivity of bipolar transistors," *IEEE Trans. Nucl. Sci.*, vol. 50, no. 6, pp. 1901–1909, Dec. 2003, doi: 10.1109/TNS.2003.821803.